SIMULATION OF HYBRID POWER SOURCES FOR INDUSTRIAL LED LIGHTING SYSTEMS

Ravindranath Tagore YADLAPALLI
Vignan University, Vadlamudi, Guntur, Andhra Pradesh,
91-9490643644, yrtagore@gmail.com.

Dr. Anuradha KOTAPATI
VNR vignana jyothi, Bachupally, Hyderabad,
91-9849542288, anuyalavarti@yahoo.co.in.

Abstract: *This paper will discuss an Air Breathing Fuel Cell (ABFC) stack and solar PV module, which are being investigated as an alternate power sources, produced from an inexhaustible sources of energy for LED lamp based industrial lighting applications. An empirical model has been developed in PSIM software in order to investigate the polarisation characteristics of the ABFC. This model includes phenomena like 'activation polarisation, ohmic polarisation, and mass transport effect'. The simulation results are also presented to consider the effect of temperature and hydrogen pressure changes on fuel cell voltage. The PV module is modelled and implemented with MPPT controller using boost converter, the P-V and I-V characteristics are presented. This paper will give focus on boost converter and the quadratic buck converter (QBC), as an ABFC stack power conditioning units (PCU) which are designed and simulated using PSIM Software. The objective is to achieve tight regulation of the LED current and should operate over a wide range of input voltages. The boost converter is implemented with sliding-mode (SM) current controller and the QBC with average current-mode (ACM) controller to achieve good line regulation as well as dynamic performance.*

Key words: *Air breathing fuel cell (ABFC), power conditioning unit (PCU), quadratic buck converter (QBC), average current-mode (ACM) controller, sliding-mode (SM) current controller.*

1. Introduction

Fuel cell is an electro chemical device which converts fuel and oxidant into DC electricity [1]. Fuel cell is characterised by high electrical efficiency and zero/low pollutant emission. Only water, heat and electricity are the products of electrochemical reaction in the fuel cell. Cells that take up oxygen, for the cathode reaction, from ambient air by passive means are known as "air-breathing" fuel cells [2]-[8]. In the ABFC, hydrogen and oxygen are fed at anode and cathode respectively as reactants. The electrons transfer from the anode to the cathode through the external circuitry of the fuel cell. Hydrogen ions transfer across the membrane internally from the anode to the cathode to complete the current flow.

Anode side reaction:

$$H_2 \rightarrow 4H^+ + 4e^-$$

Cathode side reaction:

$$O_2 + 4H^+ + 4e^- \rightarrow 2H_2O$$

Overall reaction:

$$2H_2 + O_2 \rightarrow 2H_2O + \text{Electricity} + \text{Heat}$$

Fig. 1 shows the work process and reaction principle of an ABFC.

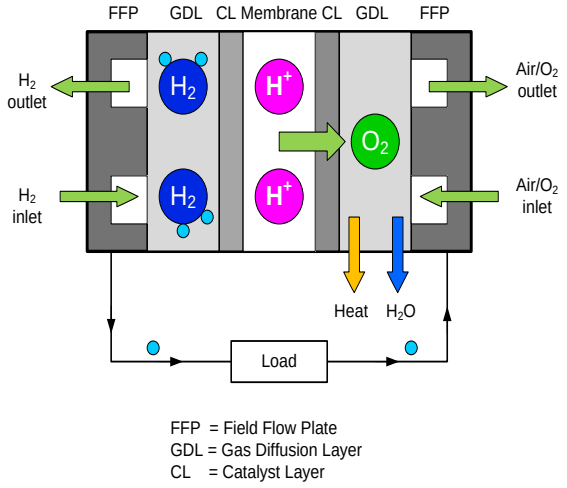

Fig. 1 - Work process and reaction principle of an ABFC

The growing interest in non-conventional sources of energy has caused the photo-voltaic (PV) power market to expand rapidly, the designers need a pliant and reliable tool to accurately track the electrical power produced from PV arrays of various sizes. A cell is defined as the semiconductor device that converts sunlight into electricity. A PV module refers to a number of cells connected in series and in a PV array the modules are connected in series and parallel.This paper presents the simulation of hybrid power sources for industrial LED lighting system. Now a day's LED lamps are becoming very popular in many applications which include outdoor spaces, hospitals, offices, automotive display systems and industrial lighting. They have high efficiency, higher durability and smaller size. As LED lamp arrays operate at different ranges of voltages and currents, they should be connected through AC-DC and DC-DC converters to the supply lines.

The switched-mode power supplies (SMPS) are extensively used as power conditioning units for fuel cell applications due to their compactness and efficiency. The existing DC-DC converters like buck converter and multi-phase buck converter are not suitable for large conversion ratios due to limitation in minimum turn-on time requirement of the switch. This limits their operation to lower switching frequencies [9]-[10]. For such requirenents the quadratic buck converter (QBC)is the preferable one compared to the other as the dc conversion ratio has a quadratic dependence on duty cycle.

The organization of this paper, section 2 presents the in-depth view of ABFC and PV module power system, section 3 describes the simulation results, efficiency analysis is described in section 4 and finally in section 5 conclusions are stated.

2. Modelling of ABFC and PV module power system

The power system model implemented in PSIM software consists of the following sections:

- ABFC stack model
- PV-module modelling
- Boost converter and the QBC

The proposed schematic of the overall power system is shown in Fig. 2.

2.1. Development of ABFC stack model

The analytical model [5]-[8] of the ABFC can be represented by a set of mathematical equations. Gibbs free energy (Δg) is the net electrical work done by the system and is expressed in terms of the enthalpy of formation, temperature and the entropy of formation represented by Eq. (1).

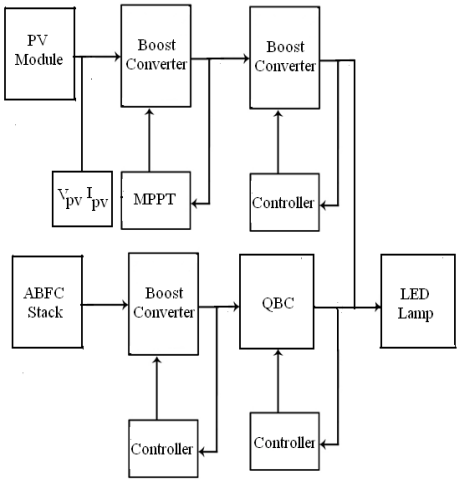

Fig. 2 - Schematic of ABFC and PV module power system

$$\Delta g = \Delta h - T\Delta s \tag{1}$$

For a fuel cell, the change in the enthalpy of formation and the change in entropy were modelled according to the mathematical Eqs. (2) and (3).

$$\Delta h = h_{H_2 0} - h_{H_2} - \frac{1}{2} h_{O_2} \tag{2}$$

$$\Delta s = s_{H_2 0} - s_{H_2} - \frac{1}{2} s_{O_2} \tag{3}$$

However, h and s are expressed as functions of temperature as represented by Eqs. (4) - (5).

$$h_T = h_{298.15} + \int_{298.15}^{T} c_p dT \tag{4}$$

$$s_T = s_{298.15} + \int_{298.15}^{T} \frac{1}{T} c_p dT \tag{5}$$

The molar specific heat at constant pressure (C_p) for steam, hydrogen and oxygen, respectively are given by the mathematical Eqs. (6) - (8).

$$c_{pSteam} = 143.05 - 58.04T^{0.25} + 8.2751T^{0.5} - 0.036989T \tag{6}$$

$$c_{pHydrogen} = 56.505 - 22222.6T^{-0.75} + 116500T^{-1} - 560700T^{-1.5} \tag{7}$$

$$c_{pOxygen} = 37.432 - 2.0102(10^{-5})T^{1.5} + 17850T^{-1.5} - 2368800T^{-2} \tag{8}$$

It is assumed that pure hydrogen and oxygen are used as reactants (i.e. $\gamma = \beta = 1$). The adopted equations which describe Activation losses, Ohmic losses, and Concentration losses respectively are represented by Eqs. (11) - (13).

The standard potential of a hydrogen/oxygen fuel cell at standard STP (25°C and 1 atm) is 1.229V. The activation losses, ohmic losses, and concentration losses are three types of irreversible losses present in the ABFC, due to which the actual cell potential drops from its equilibrium potential. The output voltage of the single cell ABFC is given by Eqs. (9) and (10).

$$V_{Cell} = E_{nernst} - \Delta V_{Act+crossover} - \Delta V_{Ohm} - \Delta V_{conc} \quad (9)$$

$$E_{nernst} = \frac{-\Delta g}{2F} + \frac{RT}{2F}\ln\left(\frac{\gamma\beta^{\frac{1}{2}}}{\delta}p^{\frac{1}{2}}\right) \quad (10)$$

It is assumed that pure hydrogen and oxygen are used as reactants (i.e. $\gamma = \beta = 1$). The adopted equations which describe Activation losses, Ohmic losses, and Concentration losses respectively are represented by Eqs. (11) - (13).

$$\Delta V_{act+fuelcrossover} = \frac{RT}{2\alpha F}\ln\left(\frac{i+i_n}{i_0}\right) \quad (11)$$

$$\Delta V_{ohm} = ir \quad (12)$$

$$\Delta V_{con} = m\exp(ni) \quad (13)$$

The block diagram of the ABFC stack is shown in Fig. 3.

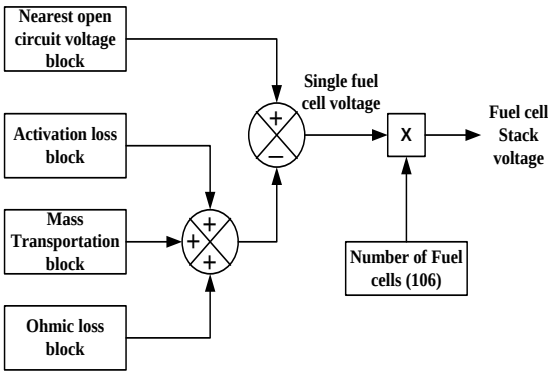

Fig. 3 - Block diagram representation of single cell behaviour under steady state conditions

The standard/Nernst potential of a hydrogen/oxygen fuel cell at standard STP (25°C and 1 atm) is 1.229V with liquid water as product. However, due to irreversible losses the actual cell potential drops from its equilibrium potential. In practice due to the irreversible losses present in ABFC viz. fuel crossover losses, electron crossover losses, activation losses, ohmic losses, and concentration losses. The theoretical efficiency of an ABFC at equilibrium potential is 83% is found by Eq. (14).

$$\eta_{FC} = \frac{V_{Cell}}{1.482} \quad (14)$$

2.2. Power conditioning unit (PCU)

2.2.1. Boost converter with SM current controller

A boost converter is a DC to DC converter whose output voltage is greater than its input voltage. Fig. 4 shows the schematic of the boost converter and its input-output voltage relation is given by Eq. (15).

$$V_0 = \frac{V_S}{(1-D)} \quad (15)$$

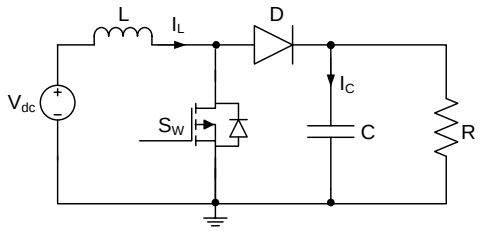

Fig. 4 - Schematic of boost converter

The sliding-mode (SM) current controller design consists of a switching function and selection of a control law [11]-[13]. The proposed SM current controller employs both the output voltage error and the input inductor-current error as controlled state variables like conventional PWM current mode control.

The instantaneous reference-inductor-current profile i_{ref} in the proposed controller is generated using the amplified output-voltage error and is given by Eq. (16).

$$i_{ref} = k(V_{ref} - \beta V_0) \quad (16)$$

Where V_{ref} and V_0 denote the reference and instantaneous output voltages respectively and K is the amplified gain of the voltage error. Large value of K is preferred to improve the dynamic response and minimizing the steady-state voltage error in the system. The switching function is given by Eq. (17).

$$u = 1/2(1+\text{sign}(s)) \quad (17)$$

Where u represents the logic state of power switch S_W and s is the instantaneous state variable's trajectory, represented by Eq. (18).

$$s = \alpha_1 x_1 + \alpha_2 x_2 + \alpha_3 x_3 \quad (18)$$

Where α_1, α_2 and α_3 represents the sliding coefficients.

The adopted controlled state variables are the current error x_1, the voltage error x_2 and the integral of the

current and the voltage errors x_3, which are expressed as

$$\left.\begin{aligned} x_1 &= (i_{ref} - i_{L_1}) \\ x_2 &= (V_{ref} - \beta V_0) \\ x_3 &= \int (i_{ref} - i_{L_1})dt + \int (V_{ref} - \beta V_0)dt \end{aligned}\right\} \quad (19)$$

The equivalent-control signal for the SM current controller is obtained by solving

$$\dot{s} = 0$$

The equivalent-control signal is obtained as

$$u_{eq} = 1 - (\frac{K_2}{V_O})i_c + K_1 \frac{(V_{ref} - \beta V_0)}{V_O} - (\frac{V_{in}}{V_o}) - K_3(\frac{i_L}{V_{in}}) \quad (20)$$

where

$$K_1 = \frac{\alpha_3}{\alpha_1} L(K+1), K_2 = \frac{\beta L}{C}(K + \frac{\alpha_2}{\alpha_1}), K_3 = (\frac{\alpha_3}{\alpha_1})L;$$

Fig. 5 shows the schematic of the boost converter with sliding-mode current controller.

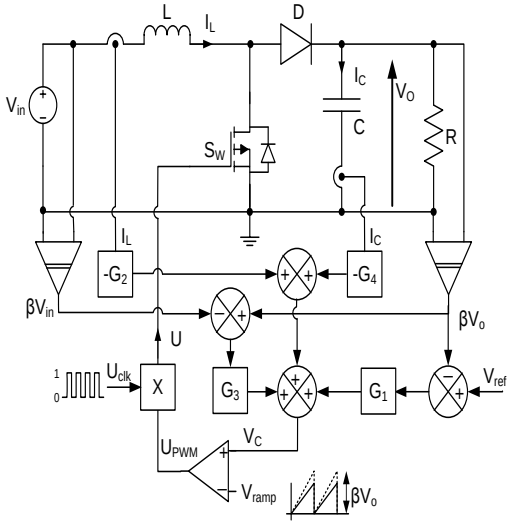

Fig. 5 - Schematic of boost converter with SM current controller

2.2.2. Quadratic buck converter (QBC)

The schematic of the quadratic buck converter is shown in Fig. 6. The conversion ratio of the QBC is represented by the Eq. (21).

$$M(D) = \frac{V_0}{V_{in}} = D^2 \quad (21)$$

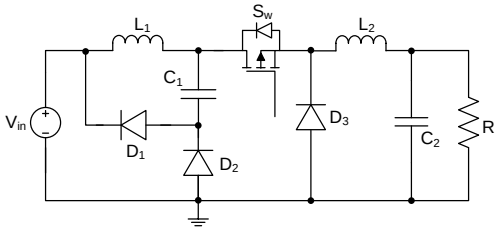

Fig. 6 - Quadratic buck converter

For a quadratic buck converter operating in continuous conduction mode, the control-output voltage transfer function has two complex right hand plane (RHP) zeros. These RHP zeros restrict the control bandwidth and cause sluggish response particularly with voltage mode controllers. The narrow gain-bandwidth limitation of the voltage-mode controller can be overcome with average current-mode controller [14]-[17]. For this, an inner current loop is used in addition to the outer voltage loop. The average current-mode control has several improved features over the peak current mode control such as large noise margin, no additional slope compensation and easy current limit implementation. The block diagram representation of QBC with average current-mode (ACM) control is shown in Fig. 7.The compensator of the current loop is designed in such a way that the crossover frequency of the current loop is greater than the voltage loop [14].

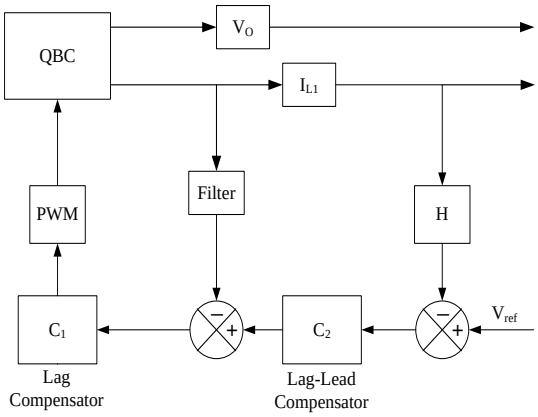

Fig. 7 - Block diagram of QBC with ACM controller

$C_1(S)$ is a lag compensator with its zero located at low frequency resonant pole. The gain of the current loop should be increased such that it adds damping to the low frequency complex poles and is represented by Eq. (22).

$$C_1(S) = \frac{K(S + Z_1)}{S} \quad (22)$$

For current loop low pass filter the corner frequency must be equal to switching frequency and its transfer function is given by Eq. (23).

$$F(S)=\left(\frac{w}{S+w}\right) \quad (23)$$

For getting stable closed loop performance, the gain crossover frequency should be very large i.e. less than 1/6 th of the converter switching frequency. The phase margin at the cross over frequency should be maintained above 30^{o}.The compensator $C_2(s)$ is to be designed for fulfilling the above requirements. The $C_2(s)$ is a lag-lead compensator whose transfer function is represented by Eq. (24).

$$C_2(S)=\frac{K(S+Z_1)(S+Z_2)}{S(S+P)} \quad (24)$$

2. 3. Photovoltaic Module

The solar cell is a non-linear device and can be represented as a current source in parallel with diode [18]-[22] as shown in the Fig. 8.

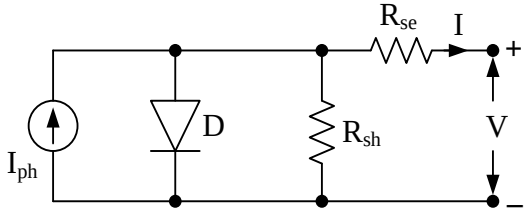

Fig. 8 - Equivalent circuit of PV cell

The current source I_{ph} represents the cell photocurrent. The R_{sh} and R_{se} are the intrinsic shunt and series resistances of the cell. Usually the value of R_{sh} is very large and R_s is very small. The module photo current is given by Eq. (25).

$$I_{ph}=\left[I_{scr}+K_i\left(T-298\right)\right]*\frac{\lambda}{1000} \quad (25)$$

The module reverse saturation current is given by

$$I_{rs}=I_{scr}/\left[\exp\left(qv_{oc}/N_skAT\right)-1\right] \quad (26)$$

The module saturation current I_o vary with the cell temperature and is given by Eq. (27).

$$I_0=I_{rs}\left[\frac{T}{T_r}\right]^3\exp\left[\frac{q*E_{go}}{Bk}\left\{\frac{1}{T_r}-\frac{1}{T}\right\}\right] \quad (27)$$

The current output of PV module is represented by

$$I_{pv}=N_p*I_{ph}-N_p*I_o\left[\exp\left\{q*(V_{PV}+I_{PV}R_S)/N_sAkT\right\}-1\right] \quad (28)$$

The output voltage obtained from the PV module is given as input to the MPPT boost converter. The second boost converter connected at the output of MPPT converter acts as a PCU for the PV source and controls the unregulated output voltage of the MPPT boost converter, maintains constant LED lamp voltage. Hence this converter can provide line voltage regulation as well as tight LED current regulation.

2.3.1. Maximum power point tracking (MPPT) controller

The Perturb & Observe (P&O) is one of the MPPT techniques and easy to implement. The time complexity of this algorithm is very less but on reaching very close to the MPP it doesn't stop at the MPP and keeps on perturbing on both the directions. When this happens the algorithm has reached very close to the MPP and we can set an appropriate error limit or can use a wait function which ends up increasing the time complexity of the algorithm. The MPPT principle and its flowchart are shown in Fig. 9 and Fig. 10 respectively.

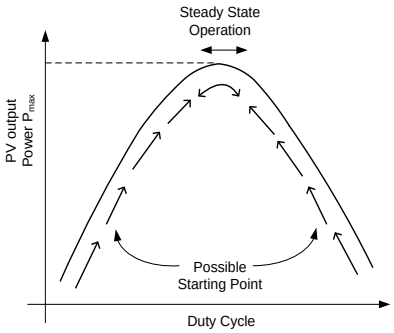

Fig. 9 - The principle of P&O MPPT strategy

The Perturb & Observe algorithm states that when the operating voltage of the PV panel is perturbed by a small increment, if the resulting change in power ΔP is positive, then it gives the direction of MPP, hence the duty cycle (δ) of the MPPT boost converter has to be incremented and keeps on perturbing in the same direction. If ΔP is negative, it gives away from the direction of MPP and the sign of perturbation supplied has to be changed, hence the duty cycle (δ) of the MPPT boost converter has to be decremented. The ΔP zero represents the maximum power point.

Two parameters needed to be designed carefully to achieve fast tracking of maximum power point with P&O MPPT algorithm. One of them is the time interval between iterations while another one is the step size of each voltage perturbation. The large step size ΔV_{PV} leads to fast tracking of the maximum power point under varying atmospheric conditions yet results in reduced overall average power conversion in steady state due to

large oscillations around the maximum power point. Likewise, the design of time interval between iterations should leave enough operating time for computer calculation, but if the time interval is designed too long, the MPPT algorithm will lose the fast response capability to a varying environmental condition.

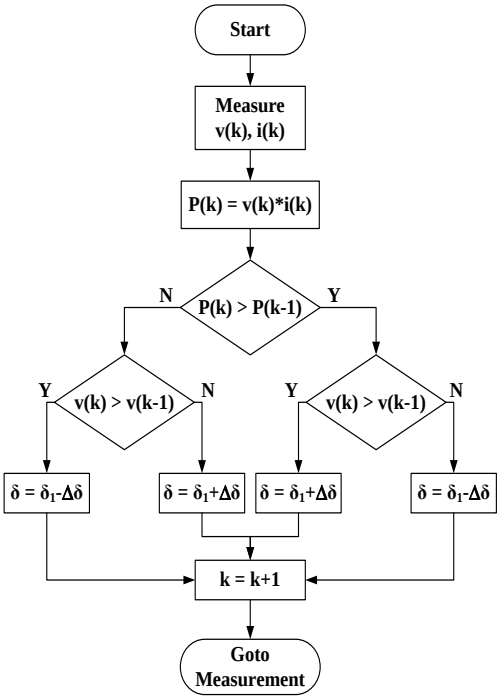

Fig. 10 - Flow chart of the P&O method

3. Simulation results

3.1. Simulation results of the ABFC power system

The ABFC stack model built in PSIM software based on block diagram of Fig. 3 is shown in Fig. 11(a)-11(d), consists of Activation loss block, Mass transportation block, Ohmic loss block and Nernst open circuit voltage block.

Table 1: Simulation parameters of ABFC model

Parameter	Value
m	0.00003 V
n	0.008 $cm^2\ mA^{-1}$
r	0.0002 KΩ cm^2
i_n	3 $mAcm^{-2}$
i_o	1 $mAcm^{-2}$
α	0.25

The values of simulation parameters adopted from the literature [5]-[8] are tabulated in Table 1. The polarisation curve is plotted for a range of current densities and at different operating temperatures of 30°C, 50°C and 60°C as shown in Fig. 12.The operating voltage of a fuel cell ranges between 0.5 and 0.6 V. According to Fig. 13, the above voltage range is produced within a current density range of approximately 40-60 mA/cm^2. Thus for the implemented model, an operating current density of 50 mA/cm^2 was selected in order to produce a reasonable operational voltage for the fuel cell. Subsequently, it was found that for a current density of 50mA/cm^2, and an exchange current density of 1 mA/cm^2, the resulting operational voltage is 0.5656V per fuel cell.

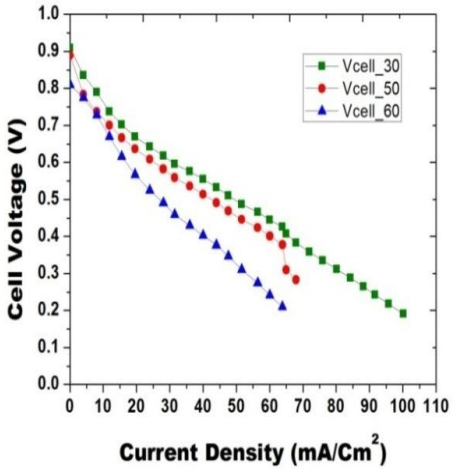

Fig. 12 - Cell voltage of an ABFC for different cell temperatures

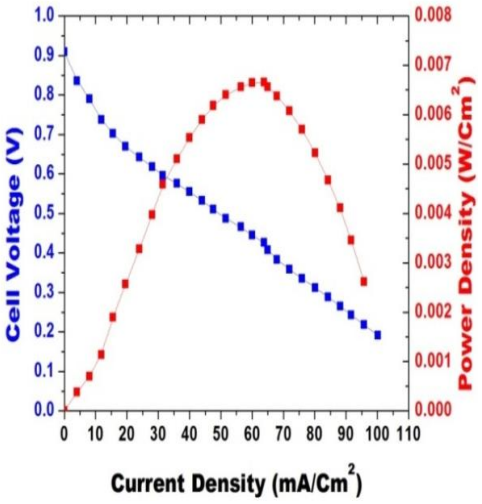

Fig. 13 - Polarization curve of an ABFC operating at 30°C

Fig. 14 presents a comparison between polarisation plots at three different cell temperatures of 30°C, 50°C, and 60°C to demonstrate the correctness of the simulation results. Theoretically, the cell voltage will be lower over the operating current density with increased cell temperature. Fig. 15 shows the output voltage of single ABFC and the fuel cell stack.

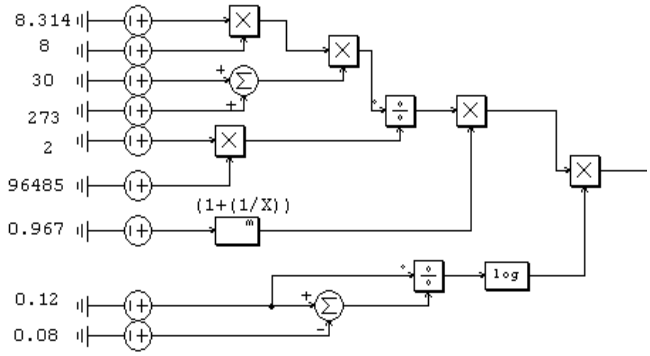

Fig. 11. (a) - PSIM model of Activation loss block

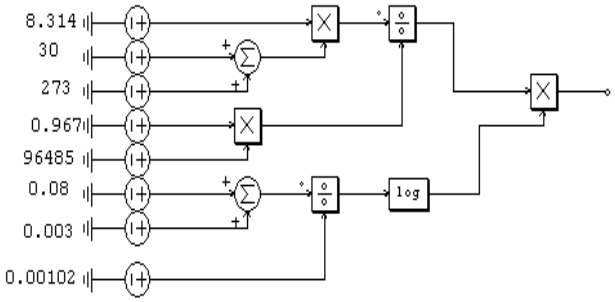

Fig. 11. (b) - PSIM model of Mass transportation block

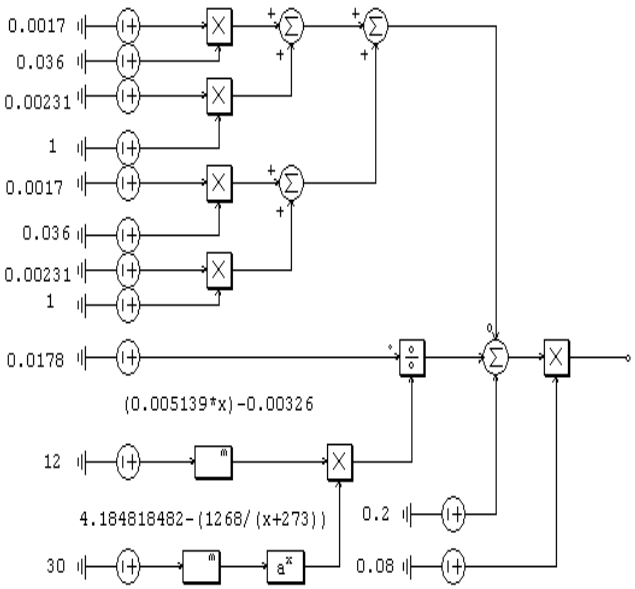

Fig. 11. (c) - PSIM model of Ohmic loss block

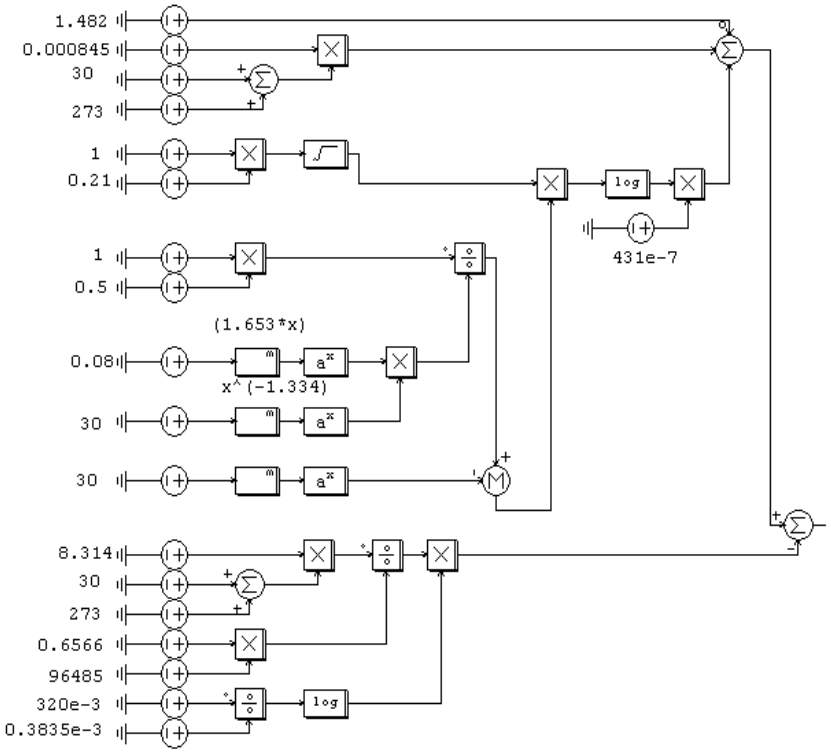

Fig. 11. (d) - PSIM model of Nernst open circuit voltage block

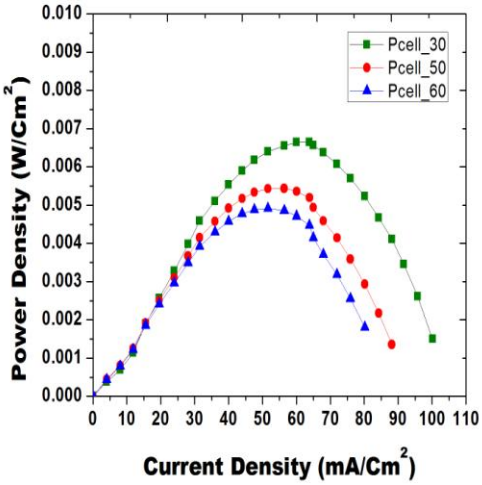

Fig. 14 - Power density curve of an ABFC for different cell temperatures

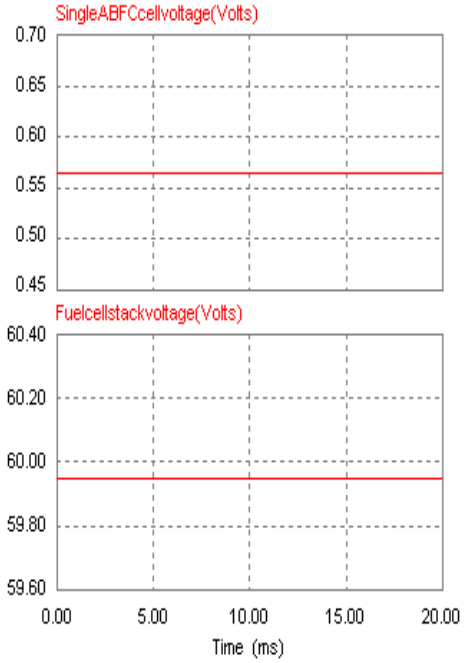

Fig. 15 - Single ABFC voltage and fuel cell stack voltage (106 cells)

At 35º each ABFC produces a voltage of 0.55V and also the fuel cell stack voltage (106 cells in series) is 58.3V. Fig. 16 shows the effect of step change in temperature (35º- 75º) on single ABFC voltage and the fuel cell stack voltage, the fuel cell voltage falls by 0.1V. Fig. 17 shows the effect of step change in pressure (1.5bar-4.5bar) on single ABFC voltage and the fuel cell stack voltage, the fuel cell voltage increases by 0.000052V.

The simulation results for temperature and pressure variations are tabulated in Table 2 and Table 3. It is evident that the change in fuel cell voltage is more with temperature compared to hydrogen pressure.

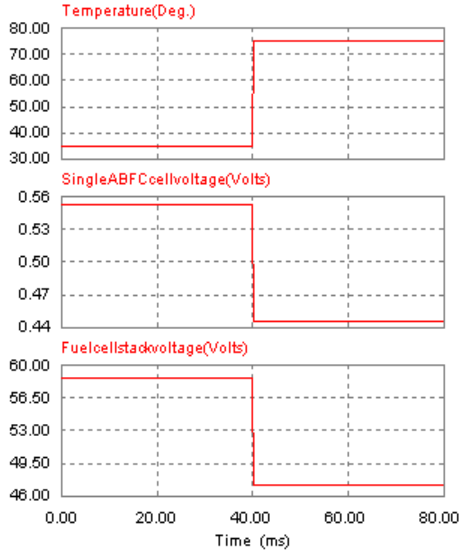

Fig. 16 - Effect of temperature change (35º- 75º) on single ABFC voltage and fuel cell stack voltage

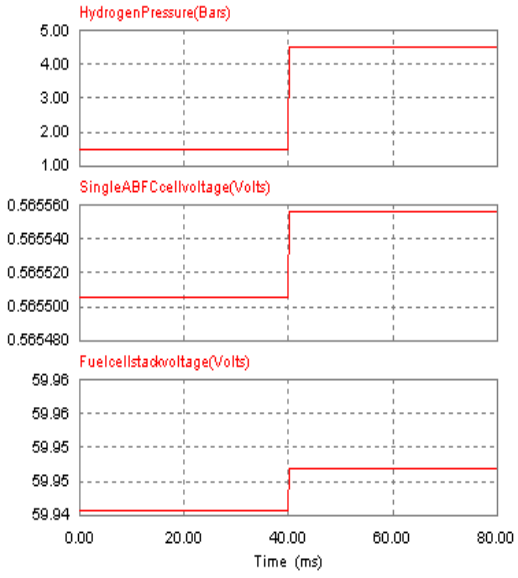

Fig. 17 - Effect of hydrogen pressure change on single ABFC voltage and fuel cell stack voltage

Table 2: Effect of step change in temperature on single ABFC voltage at constant hydrogen pressure of 4bar

Fuel cell voltage at 35º	Step change in temperature	Fuel cell voltage after step change	Decrease in fuel cell voltage
0.55V	35º - 45º	0.53V	0.02V
0.55V	35º - 55º	0.50V	0.05V
0.55V	35º - 65º	0.47V	0.08V
0.55V	35º - 75º	0.45V	0.10V

Table 3: Effect of step change in hydrogen pressure on single ABFC voltage at constant cell temperature of 35º

Step change in pressure	Fuel cell voltage before step change	Fuel cell voltage after step change	Increase in fuel cell voltage
1.5-2.5 bar	0.56550V	0.56552V	0.000022V
1.5-3.5 bar	0.56550V	0.56554V	0.000039V
1.5-4.5 bar	0.56550V	0.56555V	0.000052V

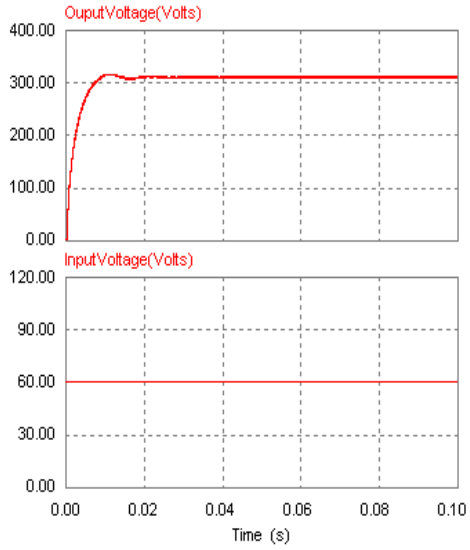

Fig. 18 - Output and stack (Input) voltage waveforms of boost converter

The output voltage (nearly 60V) obtained from the fuel cell stack model is given as input to the boost converter. The boost converter produces output voltage (311V) with a steady-state ripple of ±1V (±0.322%) as shown in Fig. 18.

3.2. Simulation parameters of QBC and Boost converter

Table 4 shows the specifications of the QBC and the LED lamp. The simulation is performed using PSIM software and the results are presented.

Table 4: Specifications of the LED lamp and quadratic buck converter

LED lamp	
Nominal voltage	170V
Nominal current	20mA
Power rating	3.4W
Quadratic buck converter	
Parameter	**Nominal value**
DC input voltage	311V
Inductance (L_1)	180mH
Inductance (L_2)	180mH
Inductive resistance	0.4mΩ
Capacitance (C_1)	1µF
Capacitance (C_2)	1µF
Capacitor (ESR)	0.2mΩ
Switching frequency	100kHz
Load resistance	8,5kΩ
Output voltage	170V
Output power	3.4W
Boost converter	
DC input voltage	60V
Inductance	0.978mH
inductive resistance	0.5mΩ
Output voltage	311V
Output power	3.4W

The bode plot for the open loop gains of current and voltage loop is shown in Fig. 19. The gain margin (GM) and phase margin (PM) for current loop are 6.22dB and 48.5°, a stable loop. Similarly for voltage loop the GM and PM 24.8dB and 49.8°. The output voltage of boost converter (311V) is given as input to the QBC, the QBC provides tight regulation of the LED current. Fig. 20 shows the output voltage and load current waveforms of the QBC with ACM controller at rated input voltage of 311V, the maximum load current deviation is 0.6mA (3.0%).

Fig. 21 shows the fuel cell stack voltage, boost converter output voltage, load voltage and load current waveforms, the output voltage is maintained constant at 170V with negligible ripple.

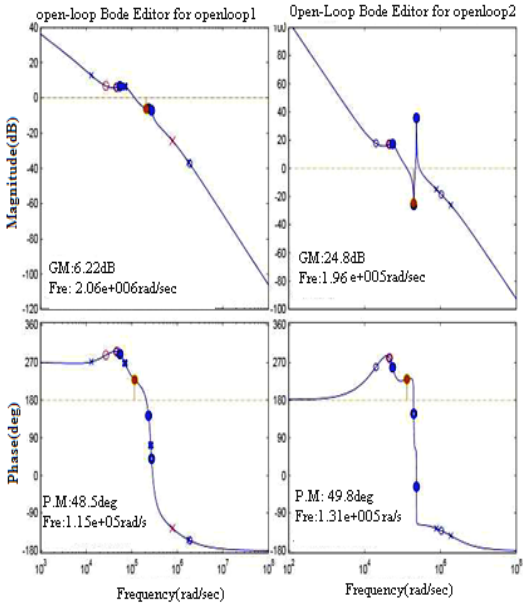

Fig. 19 - Bode plot for open-loop gains of current loop and voltage loop

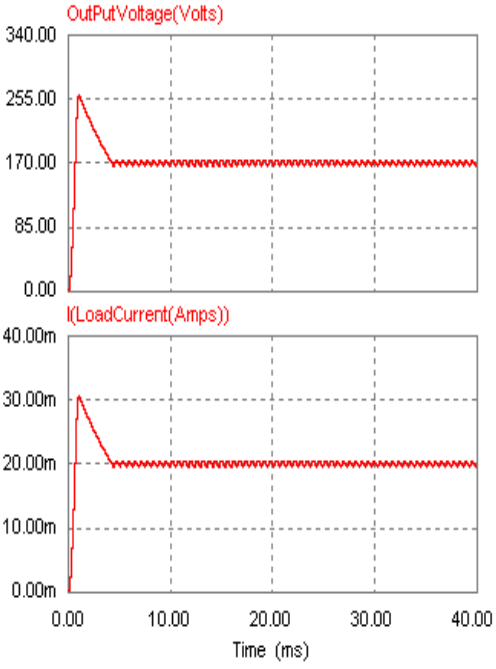

.

Fig. 20 - Output voltage and load current (LED) waveforms of QBC with ACM controller

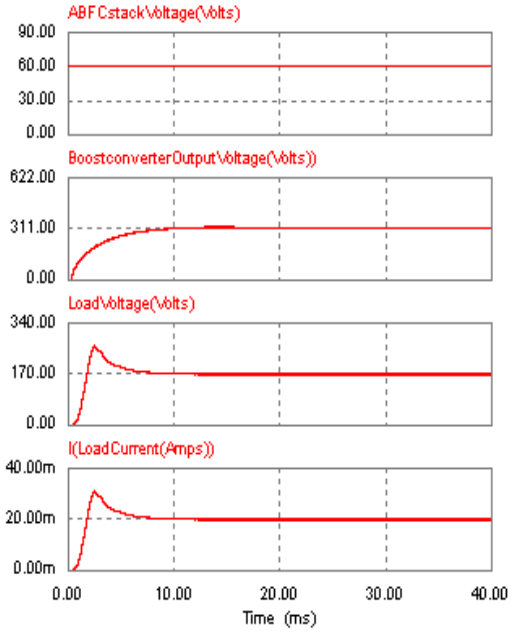

Fig. 21 - Fuel cell stack voltage, boost converter output voltage, load voltage and load current waveforms

3.3. Simulation results of PV power system

The name-plate details of the 3.4W PV module are given in Table 5.

Table 5: Electrical characteristics data of solar 3.4W PV module

Simulation parameter	Value
Rated power	3.4W
Voltage at maximum power(V_{mp})	60V
Current at maximum power(I_{mp})	0.05667A
Open circuit voltage(V_{oc})	66V
Short circuit current(I_{sc})	0.0512A
Total number of cells in series(N_s)	110
Total number of cells in parallel(N_p)	1

The PV module is implemented in PSIM software using Eqs. (25-28). The model yields the PV current I, using the electrical parameter of the module (I_{sc} ,V_{oc}, n) and the variables Voltage, Irradiation (G) and Temperature

(T) as the inputs to the model. Fig. 22 and Fig. 23 show the P-V and I-V characteristics for different irradiation levels, at constant temperature of 25°C.

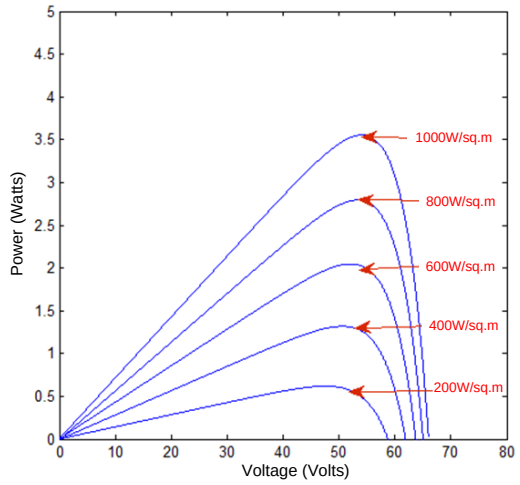

Fig. 22 - The P-V characteristics for different irradiation levels, at constant temperature of 25 ^{0} C.

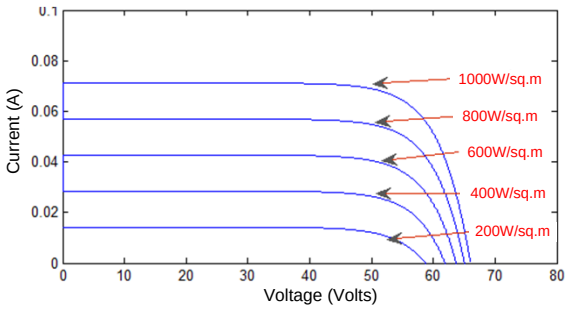

Fig. 23 - The I-V characteristics for different irradiation levels, at constant temperature of 25 ^{0} C

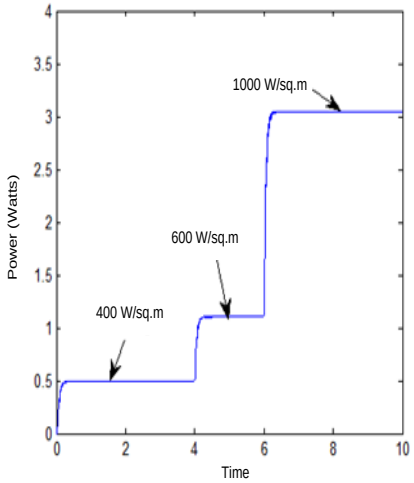

Fig. 24 - MPP Tracking for three different irradiations using P&O method

Fig. 24 shows the MPP tracking for three different irradiations, at t=4 sec the irradiance is varied from 400 W/sq.m to 600 W/sq.m and at t=6 sec the irradiance is varied from 600 W/sq.m to 1000 W/sq.m, which leads to output power rise correspondingly. The output voltage (nearly 60V) obtained from the PV module is given as input to the boost MPPT converter. This converter produces a varying intermediate voltage, the second boost converter rises this voltage to constant LED lamp voltage of 170V, provides tight regulation of the LED current.

4. Efficiency analysis

The efficiency plot of the QBC is shown in Fig. 25, the measured input power is 3.7W and the output power is 3.4W at rated input voltage of 311V, the efficiency is found to be 91.89%. The efficiency of the boost converter is also found to be 91%.

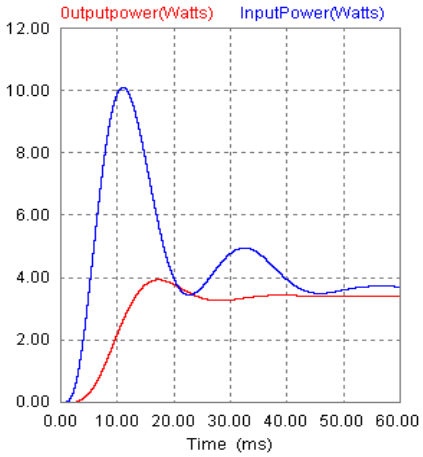

Fig. 25 - Input power and output power waveforms

The overall efficiency of the ABFC power system is found to be 69.4% (0.83*0.91*0.9189 = 0.694).

The overall efficiency of the PV module power system is found to be 27.3% (0.33*0.91*0.91 = 0.273).

5. Conclusions

In this paper a hybrid power system model is presented, includes an ABFC stack and the PV module. An empirical model of an ABFC has been developed using PSIM software in order to obtain its polarisation characteristics. The simulation model also verifies the effect of temperature and hydrogen pressure on cell voltage. At constant hydrogen pressure, as the cell temperature increases the cell voltage falls and also as hydrogen pressure increases the cell voltage increases slightly. As the output voltage of the fuel cell stack is

unregulated and often not constant, the PCU's part has been modelled and included in the overall power system model. The DC-DC converters enable tight regulation of the LED current (3.0%), besides offering a good dynamic performance. The overall efficiency of the ABFC power system is found to be 69.4%. Similarly the PV module modelling and its characteristics are also presented along with the MPPT controller. The overall efficiency of the PV power system is found to be 27.3%.

References

[1] Souleman Njoya Motapon, Olivier Tremblay, Louis A. Dessaint.: *Development of a generic fuel cell model: application to a fuel cell vehicle simulation*. In: Int. J. of Power Electronics, Vol. 4, No.6, 2012, pp. 505 - 522.

[2] J. Jia, Q. Li, Y. Wang, Y.T. Cham, M. Han.: *Modeling and Dynamic Characteristic Simulation of Proton Exchange Membrane Fuel Cell*. In: IEEE Trans. Control Syst. Technol, vol. 24, no. 16, Mar. 2009, pp. 283-291.

[3] M. Ceraolo, C. Miulli, A. Pozio.: *Modelling static and dynamic behaviour of proton exchange membrane fuel cells on the basis of electro-chemical description*. In: Journal of Power Sources, vol. 113, no. 1, 2003, pp. 131 -144.

[4] J.C.Amphlett, R. F. Mann, B. A. Peppley, P. R. Roberge, A.Rodrigues.: *A model predicting transient responses of proton exchange membrane fuel cells*. In: J. Power Sources, vol. 61, no. 1/2, Jul./Aug.2002, pp. 183-188.

[5] Kim, Jong-Soo, Choe, Gyu-Yeong, Kang, Hyun-Soo, Lee, Byoung-Kuk.: *Effect of Load Modeling on Low Frequency Current Ripple in Fuel Cell Generation Systems*. In: Journal of Electrical Engineering and Technology, vol. 5, no. 2, 2010. pp.307-318.

[6] Y. Wang and C. Y. Wang.: *Dynamics of polymer electrolyte fuel cells undergoing load changes*. In: Electrochim. Acta, vol. 51, no. 19, May 2006, pp. 3924-3933.

[7] J. C. Amphlett, M. Baumertr, F. Mannr.: *Performance modeling of the Ballard mark IV solid polymer electrolyte fuel cell: Empirical model development*. In: J. Electro chem. Soc., vol. 142, no. 1, Jan. 1995, pp. 9-15.

[8] J. Kim, M. Lees, S. Srinivasan.: *Modeling of proton exchange membrane fuel cell performance with an empirical equation*. In: J. Electro chem. Soc., vol. 142, no. 8, Aug. 1995, pp. 2670-2674.

[9] Jonas Reginaldo de Britto, Fabio Vincenzi Romualdo da Silva.: *Proposal of a DC-DC converter with wide conversion range used in photovoltaic systems and Utility power grid for the universal voltage range*. In: Power Electronics Conference, 2009, COBEP"09, pp. 606-611.

[10] Sondeep Bassan, Gerry Moschopoulos.: *Properties and applications of quadratic converters*. In: IEEE Canada Electrical Power Conference, Oct.2007, pp.123-127.

[11] Siew-Chong Tan, Y. M. Lai, C. K. Tse, Luis Martínez-Salamero, Chi-Kin Wu.: *A Fast-Response Sliding-Mode Controller for Boost-Type Converters with a Wide Range of Operating Conditions*. In: IEEE Trans. on industrial electronics, Vol. 54, No. 6, 2007, pp. 3276-3286.

[12] Yadlapalli, R.T., Kotapati, A.: *A fast-response sliding-mode controller for quadratic buck converter*. In: Int. J. Power Electronics, Vol. 6, No. 2, 2014, pp.103-130.

[13] Yadlapalli, R.T., Kotapati, A.: *An efficient sliding-mode current controller with reduced flickering for quadratic buck converter used as LED lamp driver.* In: Int. J. Power Electronics, Vol. 6, No. 4, 2014, pp.345-375.

[14] K.Karaket, C. Bunlaksananusorn.: *Modelling of a quadratic buck converter.* In: electrical engineering, electronics, computer, telecommunications and information technology (ECTI) conference, 2011, Khon Kaen, pp. 764-767.

[15] Ayachit, A j., Kazimierczuk. M. K.: *Steady-state analysis of PWM quadratic buck converter in CCM*. In: IEEE 56th international Midwest symposium, Aug, 2013, pp. 49-52.

[16] E. E. Carbajal Gutierrez, J. A. Morales Saldana, J. Leyva Ramos.: *Average Current-mode control for a quadratic buck converter*. In: Proc. IEEE Power Electron. Spec. Conf., 2005, pp. 2146-2150.

[17] Aziz Elias Demian Junior, Jonas Reginaldo de Britto.: *Microcontroller-Based Quadratic Buck Converter used as LED lamp driver*. In: Power Electronics and Applications, 2007 European Conference, pp. 1-6.

[18] Hongmei Tian, Fernando Mancilla-David, Kevin Ellis, Eduard Muljadi, Peter Jenkins.: *A Detailed Performance Model for Photovoltaic Systems*. In: Journal Article, July 2012, NREL/JA-5500-54601.

[19] S. L. Brunton, C.W. Rowley, S. R. Kulkarni, and C. Clarkson.: *Maximum power point tracking for photovoltaic optimization using ripple-based extremum seeking control*. In: IEEE Trans. Power Electron., Oct. 2010, vol. 25, no. 10, pp. 2531-2540.

[20] David Velasco de la Fuente, César L. Trujillo Rodríguez, Gabriel Garcerá, Member, Emilio Figueres, Rubén Ortega Gonzalez.: *Photovoltaic Power System With Battery Backup With Grid-Connection and Islanded Operation Capabilities*. In: IEEE Transactions on Industrial Electronics, April 2013, Vol. 60, No. 4.

[21] Ahmed A. El-Sattar, Naggar H. Saad, Nessreen. M. Rady.: *Calculation of Voltage Thresholds for Sources Scheduling in a Hybrid Renewable Nangrid*. In: Journal of Electrical Engineering (JEE), Volume 13 edition 4, p.p. 301-307.

[22] Hassan abouobaida, M. Cherkaoui.: *three phase grid-connected photovoltaic system using MPPT and back stepping-based control in a boost converter*. In: Journal of Electrical Engineering (JEE), Volume 14 edition 4, p.p 260-267.